Urban Geospatial Planning and Sustainability; Vol.3, No.1; 2026
E-ISSN: 3006-5011 P-ISSN: 3006-5003
DOI: https://doi.org/10.70267/ugps.v3n1.1625
Published by: Zeus Press

Impacts of the Urban Heat Island on Areas of Dense Human Activity— A Study Based on Blue-Green Space, Land Surface Temperature, and Weibo Activity Hotspots in Hangzhou

Yuchen Song*

Hangzhou Foreign Languages School, Hangzhou, Zhejiang, 310023, China

**Corresponding author: Yuchen Song.*

Abstract

The urban heat island is not a uniformly high-temperature zone: areas with higher temperatures are not necessarily those with the most intensive human activity, and relatively cool zones do not necessarily encompass activity hotspots. Taking Hangzhou's contiguous built-up area as the study area, this study retrieved and processed 18 Landsat 8 Collection 2 Level-2 images, of which 15 provided valid pixels within Hangzhou. A composite land surface temperature map for the summer of 2020 was then generated. Water bodies, green space, buildings, roads, and 244,718 geotagged summer Weibo posts were aggregated into 2,332 500-meter grids. Using descriptive statistics, Spearman rank-order correlation, and multiple linear regression, this paper analyzes the spatial relationships between the urban environment and land surface temperature. Upper-quartile thresholds were used to identify high-temperature and high-activity grids. The median grid-level land surface temperature was 45.9 °C. Water-body proportion was negatively correlated with land surface temperature ($\rho = -0.21$) and maintained a strong negative association after controlling for other variables (standardized $\beta = -0.33$). Building-coverage ratio was the strongest positive predictor ($\beta = 0.43$). The independent association of green-space proportion was not significant ($\beta = 0.01$, $p = 0.674$). The 189 high-temperature-high-activity grids contained 29.7 % of summer Weibo posts; among them, 106 grids with a blue-green-space proportion below the regional median contained 20.1 % of total posts. This study moves forward the classic "where is it hot?" heat-island question toward a spatial question: "Which activity sites deserve priority attention?"

Keywords

urban heat island effect, land surface temperature, blue-green space, Weibo, activity hotspots, Hangzhou

1. Introduction

On sunny summer days, roofs, roads, plazas, water surfaces, and tree-covered areas warm at different rates, creating pronounced spatial differences within cities. Roads, rooftops, and plazas absorb and store solar radiation, while reduced vegetation weakens evapotranspiration; together these processes contribute to the urban heat-island effect. Oke (1982) explained the phenomenon through the urban energy budget [1]. Thermal-infrared remote sensing provides continuous spatial coverage, but it measures land surface "skin" temperature rather than the 2-m air temperature recorded by meteorological stations [2]. Global comparisons also distinguish surface urban heat islands from air-temperature-based measures [3]. This paper does not calculate urban–rural heat-island intensity; instead, it examines internal land-surface-temperature patterns within Hangzhou's contiguous built-up zone. Hereinafter, "temperature" refers to satellite-retrieved land surface temperature.

Blue-green spaces can moderate this warming through complementary physical processes.

Vegetation shades surfaces and removes energy through evapotranspiration. Water bodies cool nearby surfaces through evaporation, high heat capacity, and local energy exchange.

Systematic reviews generally support the cooling effects of urban greenery and water bodies, although the magnitude and spatial scale vary with climate, vegetation form, water-body size, and analytical extent [4, 5, 6]. Cooling magnitudes reported for one city therefore cannot be transferred directly to Hangzhou; local data may yield different patterns.

Figure 1: Research workflow linking land surface temperature, blue-green space, and Weibo activity hotspots

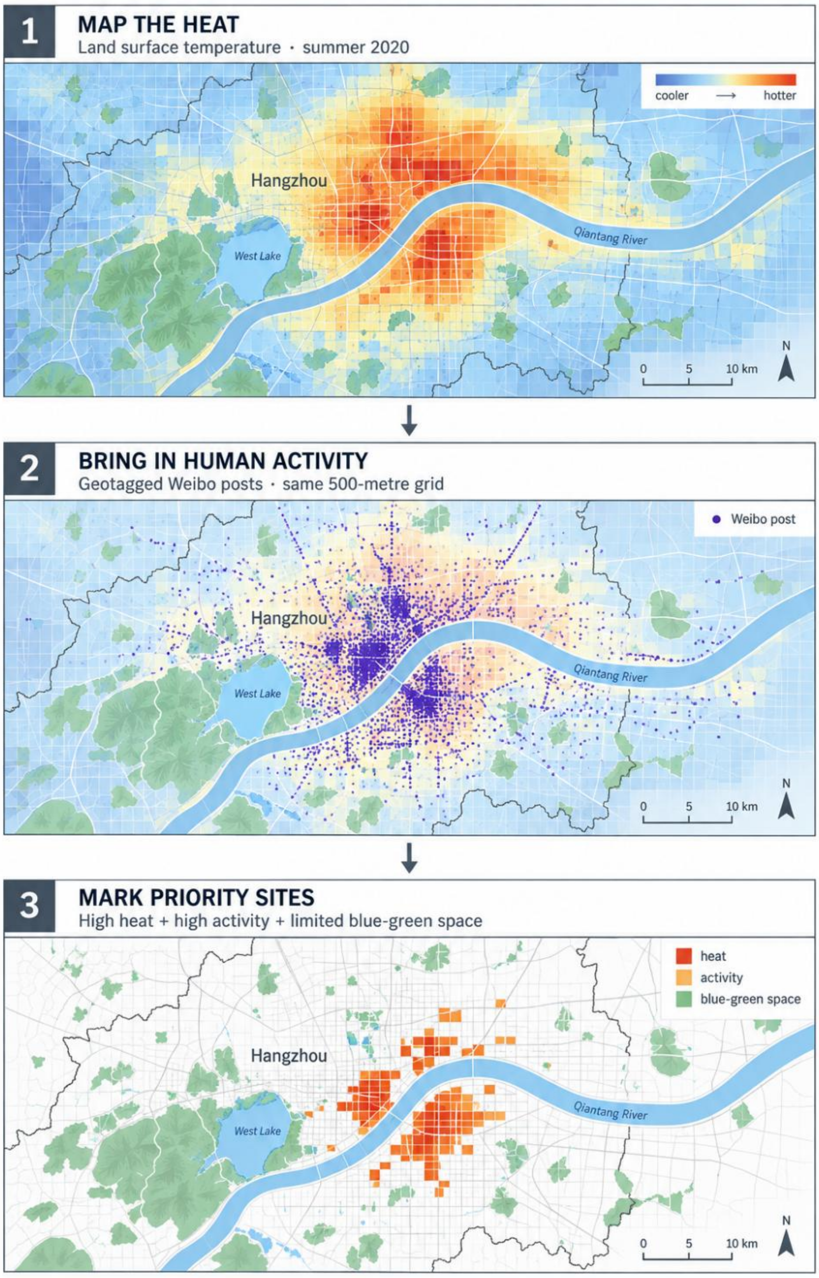

Nevertheless, mapping “where it is hot” is insufficient. Urban cooling facilities ultimately serve human activities at specific locations, while temperature maps cannot indicate the intensity of site use. Geotagged social media data offer supplementary proxies for place-based human activities [7, 8]. This study uses Weibo posting density within each grid as a proxy for activity intensity and examines spatial overlap between high-temperature zones and activity hotspots.

Three core research questions are addressed: What are the spatial differences in intra-urban land surface heat-island patterns within Hangzhou’s contiguous built-up area? What relationships exist between land surface temperature and the explanatory variables, including water bodies, green space, buildings, and roads? Which high-temperature grids simultaneously exhibit intense Weibo activity and limited blue-green space? Regular gridding, spatial overlay, correlation analysis, and multiple linear regression are applied to test these questions. The analytical workflow is summarized in Figure 1.

2. Data and Methods

2.1 Study Area and Analytical Units

Hangzhou’s administrative jurisdiction encompasses extensive mountainous terrain, rural land, and multiple dispersed towns. To reduce their interference with intra-urban relationships, the study area is restricted to contiguous built-up zones. Regular 500-meter grids were generated under the EPSG:32650 coordinate system, and the building-coverage ratio was calculated for each grid. Grids with building coverage ≥ 1 % that belonged to the largest 8-neighbor connected component were retained. The final study sample contains 2,332 grids covering approximately 583 km², geographically bounded by 119.91°–120.40° E and 30.11°–30.48° N.

2.2 Data Sources

Table 1: Datasets and Their Applications in This Study

Dataset	Scale or Resolution	Application in This Study	Main Limitations
Landsat 8 Collection 2 Level-2	18 scenes retrieved; 15 scenes yielded valid pixels across 9 valid dates; output resolution: 100 m	Summer clear-sky land surface temperature and valid observation counts	Valid dates and observation counts vary geographically
Hangzhou municipal boundary	1 municipal boundary layer	Clipping and candidate-grid generation	Administrative boundary exceeds primary study area
Baidu optimized building dataset	273,978 building polygons	Building-coverage ratio, area-weighted average building height	Metadata on data production year and height sources remain incomplete
Interpreted green-space and park polygons	183,531 green-space polygons, 3,994 park polygons	Green-space proportion	Labeled as 2023 dataset; original imagery dates and classification accuracy undocumented
Water-system and lake polygons	98 water-system polygons, 817 lake polygons	Water-body proportion; geometric merging and deduplication	Small or seasonal water bodies may be omitted
Road network	85,406 line features	Grid-level road density	Incomplete records for road grade, width, and construction year
2020 Hangzhou Weibo posts	1,339,181 city-wide posts; 244,718 summer posts within study area	Proxy for potential human-activity intensity	Only posting dates are available; no posting-time stamps or user IDs; platform representativeness is limited

Table 1 summarizes the data sources and their uses. Production years for the building, green-space, and road vector layers are not perfectly aligned. This paper analyzes spatial associations between these land-cover variables and summer 2020 land surface temperature.

2.3 Land Surface Temperature Processing

Landsat 8 Collection 2 Level-2 Tier-1 imagery covering Hangzhou between 1 June and 31 August 2020 was retrieved via the STAC interface on Microsoft Planetary Computer [9]. The scene cloud-cover threshold was set at 80 % to avoid premature elimination of locally clear-sky pixels during retrieval. After retrieval, per-pixel QA_PIXEL bits 0–5 were applied to mask fill values, dilated clouds, cirrus clouds, clouds, cloud shadows, and snow; QA_RADSAT masks removed radiometrically saturated pixels.

Land surface temperature values were derived from the official ST_B10 product using the USGS scaling formula [10, 11]:

$$\text{LST (°C)} = \text{DN} \times 0.00341802 + 149.0 - 273.15.$$

All valid pixels were reprojected onto a 100-meter grid under EPSG:32650. Per-pixel medians were computed across valid summer observations. Eighteen scenes were processed, of which 15 provided valid pixels for Hangzhou across 9 distinct dates. The composite result covers 96.3 % of Hangzhou's municipal boundary; 74.7 % of municipal pixels contain at least two valid observations, with a median observation count of 2. Missing values accounting for the remaining 3.7 % mainly stem from quality masks or Level-2 emissivity gaps.

2.4 Grid-Level Environmental Metrics

In this project, physical building, green-space, park, and water-body features were precisely intersected with 500-meter grids under metric projection. Area proportions were calculated by dividing the intersecting area by 250,000 m². Water-system and lake geometries were merged to prevent double-counting of overlapping zones. Average building height was area-weighted within each grid; nonpositive height values were excluded from averaging. Road density equals the total road length per grid divided by 0.25 km² (unit: km/km²). Grid-level summer land surface temperature is the average value of valid internal 100-meter pixels. Only grids with a valid-pixel fraction ≥ 50 % entered the analysis. All 2,332 study grids satisfied this criterion, with a median valid-pixel fraction of 100 %.

2.5 Weibo-Derived Activity Metric

The original one Weibo dataset contains 1,339,181 posts from 2020 with date, text, source, and geocoordinate attributes. Posts dated from June through August and falling within contiguous built-up zones were retained, totaling 244,718 records across 92 days. In order to reduce day-to-day fluctuations in total posting volume, each grid's daily posting fraction relative to the study-area total was calculated, then averaged over the 92-day period and converted into relative activity intensity in parts per million (ppm).

Sentiment samples include only 1,998 Weibo posts, of which only 624 are summer records. Sentiment analysis is therefore omitted; only aggregate grid-level posting counts are used to calculate activity intensity. All outputs are aggregated at the grid level; no raw Weibo texts, post identifiers, or exact point locations are displayed.

2.6 Statistical Analysis and Classification Rules

First, computations were done using descriptive statistics and Spearman rank-order correlations. Next, multiple linear regression models were fitted with grid-level land surface temperature as the dependent variable and green-space proportion, water-body proportion, building-coverage ratio, area-weighted average building height, and road density as explanatory variables. Subsequently, variables were standardized before modeling to facilitate comparison of the coefficient directions and magnitudes. HC3 robust standard errors were adopted. Adjusted R^2, variance inflation factors (VIF), and residual spatial autocorrelation were examined as model assessments.

Upper-quartile thresholds defined the classification rules: grids with land surface temperature ≥ 47.66 °C are categorized as high-temperature grids; grids with Weibo activity intensity ≥ 433.25 ppm are categorized as high-activity grids. Cross-classification yields four grid types. Within the high-temperature-high-activity grids, those whose blue-green-space proportion lies below the study-area median (25.39 %) were marked as priority candidates for further investigation. These thresholds apply only to internal comparisons within this study area.

3. Results

3.1 Spatial Patterns of Hangzhou'S Land Surface Heat Island

Across 2,332 grids, the mean summer land surface temperature is 45.8 °C, with a median of 45.9 °C; grid-level means range from 32.8 °C to 58.3 °C. Study-area summary statistics are as follows: mean green-space proportion, 27.3 %; mean water-body proportion, 2.5 %; mean building-coverage ratio, 12.2 %; area-weighted mean building height, 35.4 m; and mean road density, 13.1 km/km². The spatial distributions are shown in Figure 2.

Figure 2: Summer land surface temperature, green-space proportion, and Weibo activity intensity across 500-m grids

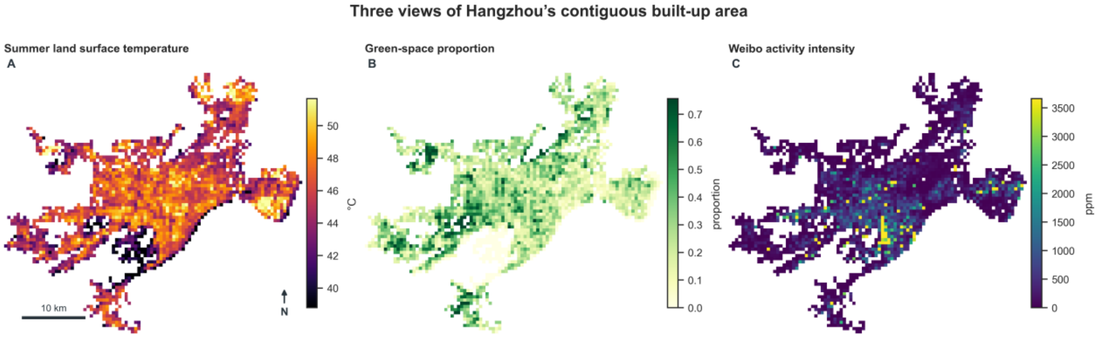

Figure 2 demonstrates that Weibo activity is concentrated primarily in the central city and several commercial and transportation-intensive zones, while high-temperature patches are more widely distributed. Spatial overlap between temperature hotspots and activity hotspots is only partial.

3.2 Bivariate Correlations

Spearman correlation results show that the building-coverage ratio exhibits the strongest positive correlation with land surface temperature ($\rho = 0.52$, $p < 0.001$). Road density shows a weak positive correlation ($\rho = 0.20$, $p < 0.001$), and water-body proportion shows a negative correlation ($\rho = -0.21$, $p < 0.001$). Weibo activity intensity is weakly positively correlated with land surface temperature ($\rho = 0.21$, $p < 0.001$), confirming that temperature and human activity must be analyzed separately. Figure 3 summarizes these pairwise and adjusted associations.

The rank-order correlation between green-space proportion and land surface temperature is weak and not significant ($\rho = -0.02$, $p = 0.321$). Average building height also shows no significant bivariate correlation ($\rho = -0.01$, $p = 0.792$). At the 500-meter analytical scale of this dataset, neither green-space proportion nor building height alone adequately explains grid-to-grid temperature variations.

Figure 3: Spearman correlations and standardized regression coefficients for land surface temperature (n = 2,332)

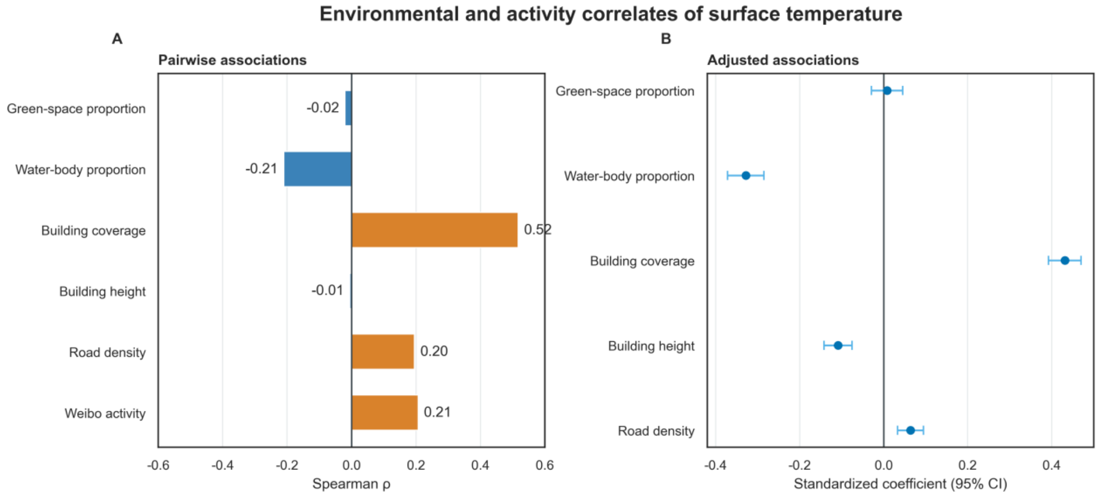

3.3 Multiple Regression Outcomes

The five explanatory variables jointly explain 35.9 % of the variance in grid-level temperature (adjusted R^2 = 0.358, overall model $p < 0.001$). The building-coverage ratio has the largest positive standardized coefficient (β = 0.431, 95 % CI [0.392, 0.470], $p < 0.001$), indicating that, holding other variables statistically constant, grids with higher building coverage generally have higher land surface temperatures. Water-body proportion has the largest negative coefficient (β = −0.328, 95 % CI [−0.371, −0.285], $p < 0.001$). Full coefficient estimates are reported in Table 2.

Average building height shows a weak negative association (β = −0.109, 95 % CI [−0.142, −0.075], $p <$ 0.001). Road density shows a small positive association (β = 0.064, 95 % CI [0.033, 0.095], $p < 0.001$). The coefficient for green-space proportion is close to zero (β = 0.008, 95 % CI [−0.029, 0.045], p = 0.674). All VIF values range from 1.01 to 1.13, indicating no severe multicollinearity.

Table 2: Multiple Linear Regression Results

Variable	Standardized β	95 % Confidence Interval	p-value	Interpretation
Green-space proportion	0.008	−0.029–0.045	0.674	No detectable independent association
Water-body proportion	−0.328	−0.371 to −0.285	< 0.001	Strong negative association
Building-coverage ratio	0.431	0.392–0.470	< 0.001	Strongest positive association
Area-weighted average building height	−0.109	−0.142 to −0.075	< 0.001	Weak negative association
Road density	0.064	0.033–0.095	< 0.001	Minor positive association

Figure 4: Green-space proportion and land surface temperature across water-body-proportion groups

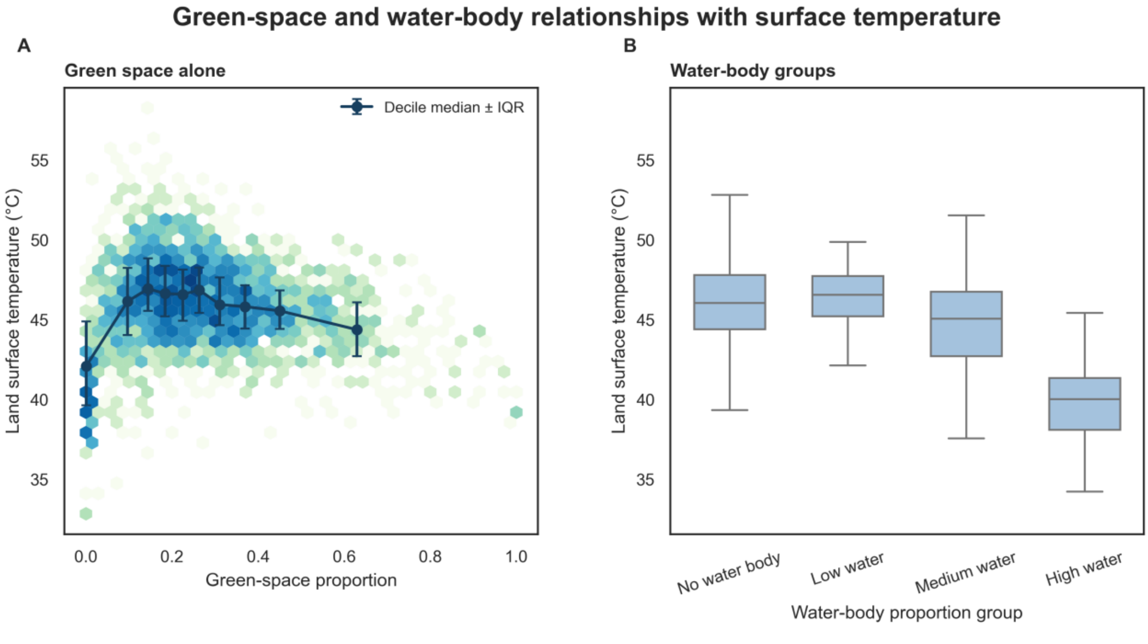

Figure 4 provides a grouped view of the distributions. Sensitivity analysis restricted to 1,704 grids with ≥ 2 valid observations returns consistent coefficient directions: water-body proportion β = −0.354, building-coverage ratio β = 0.436, average building height β = −0.131, road density β = 0.053, and green-space proportion remains near zero and not significant (β = 0.002, p = 0.923).

Model residuals reveal marked spatial autocorrelation (Moran's I = 0.557, p = 0.001 under 999 permutations). This implies that neighboring grids are jointly influenced by unmodeled factors, including surface materials, local meteorology, and block morphology. Regression outputs are therefore used primarily to compare coefficient directions and relative effect magnitudes.

3.4 Where Do High-Temperature Zones and Activity Hotspots Intersect?

Quartile-based cross-classification yields 189 high-temperature-high-activity grids, accounting for 8.1 % of all grids and hosting 29.7 % of summer Weibo posts. The 394 low-temperature-high-activity grids and 394 high-temperature-low-activity grids contain 51.9 % and 4.7 % of total posts, respectively. The four groups are summarized in Table 3, and their spatial overlap is shown in Figure 5.

Table 3: Four grid types stratified by temperature and Weibo activity intensity

Type	Number of Grids	Mean Land Surface Temperature (°C)	Fraction of Summer Weibo Posts
Low-temperature-low-activity	1,355	44.5	13.7 %
Low-temperature-high-activity	394	45.0	51.9 %
High-temperature-low-activity	394	49.4	4.7 %
High-temperature-high-activity	189	49.0	29.7 %

Figure 5: Overlap of high-temperature and high-activity grids; black outlines mark low-blue-green-space priority candidates

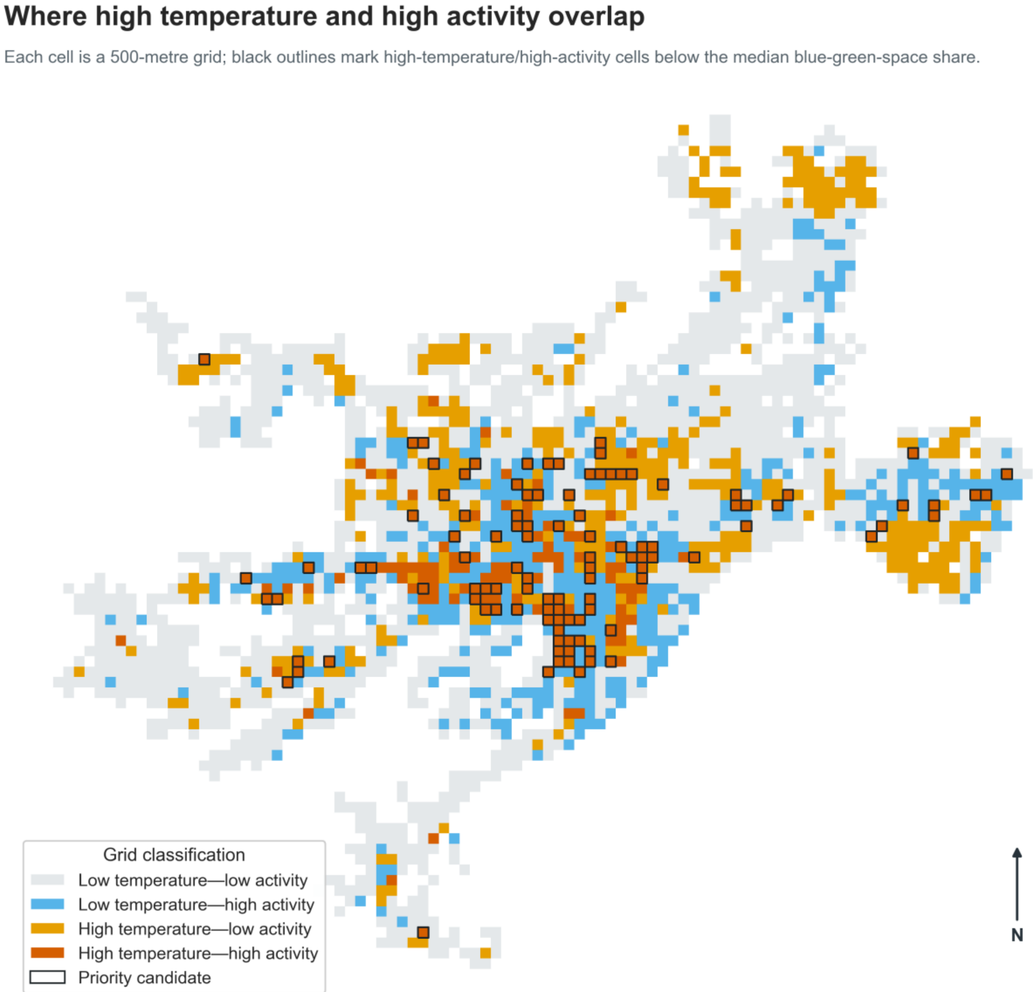

Within the 189 high-temperature-high-activity grids, 106 grids have a blue-green-space proportion below the 25.39 % regional median. These priority candidate grids represent 4.5 % of total grids and contain 20.1 % of summer Weibo posts.

4. Discussion

4.1 Blue-Green Space and Heat-Island Patterns

Noticeable spatial differentiation characterizes land surface temperature across Hangzhou's contiguous built-up zone. The building-coverage ratio correlates positively with elevated temperatures, while water-body proportion correlates negatively. Notably, green-space proportion shows no detectable independent negative association. This result may reflect the green-space dataset's inability to distinguish tree canopy from grassland, the mismatched production years among vector layers, and land-cover mixing within 500-m grids. Studies that explicitly represent tree canopy often find stronger and more spatially variable cooling effects [13, 14], so finer canopy data are needed for a direct test [12].

Results for water bodies correspond to the conclusions of previous research [5]. West Lake, the Qiantang River, and urban river networks provide abundant surface water in Hangzhou, yet most grids contain zero water-body coverage; the findings mainly contrast water-containing grids with ordinary built-up grids. Further investigations may differentiate rivers, lakes, and small-scale water surfaces and analyze distance-decay effects from large water bodies.

Positive associations for the building-coverage ratio accord with physical explanations of heat absorption by impervious surfaces. After controlling for the building-coverage ratio, average building height correlates negatively with temperature. This pattern may originate from shadows created by buildings or compact development patterns; it may also be confounded by the quality of the building-height data and urban location. Since rooftop material, albedo, and street-canyon geometry are not directly measured, this result cannot be interpreted solely as a cooling effect of taller buildings.

4.2 From Temperature Mapping to Human-Activity Locations

Weibo-derived activity data provide site-use information unavailable from temperature maps alone. The 189 high-temperature-high-activity grids host nearly 30 % of summer Weibo posts. Superimposing temperature and activity layers narrows the scope of investigation to locations that are both hot and heavily used.

Because user identifiers and reliable intraday timestamps are unavailable, Weibo post fractions reflect only spatial posting distributions and cannot quantify population counts or synchronous heat exposure. Platform-user demographics, tourism volume, commercial-site distribution, and posting conventions bias spatial outputs [15, 8, 16].

4.3 Locations Justifying Further Field Investigation

The 106 grids characterized by low blue-green coverage, high temperature, and high human-activity intensity constitute priorities for field surveys. Fieldwork could focus on pedestrian walkways, bus stops, and commercial plazas with heavy foot traffic, documenting shade conditions, hard paving, and tree-canopy continuity. For candidate grids adjacent to rivers or lakes, field surveys should assess accessibility to waterfront zones and shade deficiency along shorelines. Specific mitigation interventions must be customized to on-site conditions.

4.4 Study Limitations

Landsat-retrieved land surface temperature captures surface conditions at satellite overpass times under clear-sky weather; these measurements differ from all-day air temperature and measures of human thermal comfort [17]. Effective observation counts vary across dates and orbital tracks; summer median compositing mitigates single-scene stochasticity, yet weather variation and orbital seams may persist within composite outputs. Mixed land-cover signals exist within 100-meter pixels, precluding building-scale analysis.

Incomplete metadata on the production years and accuracy of the green-space, building, and road vector layers introduce a temporal mismatch that may distort statistical relationships. The study area is filtered by building-coverage thresholds; regression coefficients for the building-coverage ratio are valid only within this defined domain. Weibo datasets suffer biases originating from platform-user composition, tourism, and location-dependent posting behaviors. Pronounced geographical clustering in regression residuals indicates the omission of covarying local predictors for neighboring grids. The findings are therefore suited primarily to describing spatial relationships and screening candidate investigation sites.

5. Conclusions

Based on 18 Landsat scenes and a 500-meter gridded analysis, this paper studies summer land surface heat-island patterns inside Hangzhou's contiguous built-up area. Grids with a larger water-body proportion usually exhibit cooler surface heat levels, whereas grids with a higher building-coverage ratio tend toward hotter conditions. Green-space proportion shows no statistically significant independent negative association; this result awaits reexamination with higher-resolution tree-canopy classification and more accurate vector datasets.

Weibo-identified activity hotspots do not perfectly coincide with temperature hotspots. By combining both datasets, grids featuring high temperature, intensive human activity, and scarce blue-green amenities are identified. These grids serve as priority targets for subsequent field-based investigations.

References

[1] Oke, T. R. (1982). The energetic basis of the urban heat island. Quarterly Journal of the Royal Meteorological Society, 108(455), 1–24. https://doi.org/10.1002/qj.49710845502

[2] Voogt, J. A., & Oke, T. R. (2003). Thermal remote sensing of urban climates. Remote Sensing of Environment, 86(3), 370–384. https://doi.org/10.1016/S0034-4257(03)00079-8

[3] Peng, S., et al. (2012). Surface urban heat island across 419 global big cities. Environmental Science & Technology, 46(2), 696–703. https://doi.org/10.1021/es2030438

[4] Bowler, D. E., Buyung-Ali, L., Knight, T. M., & Pullin, A. S. (2010). Urban greening to cool towns and cities: A systematic review of the empirical evidence. Landscape and Urban Planning, 97(3), 147–155. https://doi.org/10.1016/j.landurbplan.2010.05.006

[5] Gunawardena, K. R., Wells, M. J., & Kershaw, T. (2017). Utilising green and bluespace to mitigate urban heat island intensity. Science of the Total Environment, 584–585, 1040–1055. https://doi.org/10.1016/j.scitotenv.2017.01.158

[6] Ziter, C. D., Pedersen, E. J., Kucharik, C. J., & Turner, M. G. (2019). Scale-dependent interactions between tree canopy cover and impervious surfaces reduce daytime urban heat during summer. Proceedings of the National Academy of Sciences, 116(15), 7575–7580. https://doi.org/10.1073/pnas.1817561116

[7] Cao, Z., et al. (2020). Explicit spatializing heat-exposure risk and local associated factors by coupling social media data and automatic meteorological station data. Environmental Research, 188, 109813. https://doi.org/10.1016/j.envres.2020.109813

[8] Wang, J., et al. (2021). Mapping the exposure and sensitivity to heat wave events in China's megacities. Science of the Total Environment, 755, 142734. https://doi.org/10.1016/j.scitotenv.2020.142734

[9] Ermida, S. L., Soares, P., Mantas, V., Göttsche, F.-M., & Trigo, I. F. (2020). Google Earth Engine open-source code for land surface temperature estimation from the Landsat series. Remote Sensing, 12(9), 1471. https://doi.org/10.3390/rs12091471

[10] U.S. Geological Survey. (2021). Landsat Collection 2 Surface Temperature. https://www.usgs.gov/landsat-missions/landsat-collection-2-surface-temperature

[11] U.S. Geological Survey. (2021). How do I use a scale factor with Landsat Level-2 science products? https://www.usgs.gov/faqs/how-do-i-use-a-scale-factor-with-landsat-level-2-science-products

[12] Weng, Q., Lu, D., & Schubring, J. (2004). Estimation of land surface temperature–vegetation abundance relationship for urban heat island studies. Remote Sensing of Environment, 89(4), 467–483. https://doi.org/10.1016/j.rse.2003.11.005

[13] Li, Y., et al. (2024). Green spaces provide substantial but unequal urban cooling globally. Nature Communications, 15, 7108. https://doi.org/10.1038/s41467-024-51355-0

[14] Schwaab, J., et al. (2021). The role of urban trees in reducing land surface temperatures in European cities. Nature Communications, 12, 6763. https://doi.org/10.1038/s41467-021-26768-w

[15] Martí, P., Serrano-Estrada, L., & Nolasco-Cirugeda, A. (2019). Social media data: Challenges, opportunities and limitations in urban studies. Computers, Environment and Urban Systems, 74, 161–174. https://doi.org/10.1016/j.compenvurbsys.2018.11.001

[16] Lyu, F., Zhou, L., Park, J., Baig, F., & Wang, S. (2024). Mapping dynamic human sentiments of heat exposure with location-based social media data. International Journal of Geographical Information Science, 38(7), 1291–1314. https://doi.org/10.1080/13658816.2024.2343063

[17] Kuras, E. R., et al. (2017). Opportunities and challenges for personal heat exposure research. Environmental Health Perspectives, 125(8), 085001. https://doi.org/10.1289/EHP556

Funding

This research received no external funding.

Conflicts of Interest

The authors declare no conflict of interest.

Acknowledgment

This paper is an output of the science project.

Copyrights